

Non-Linear Least-Squares Reverse-Time Migration

Gang Yao* and Helmut Jakubowicz, Imperial College London

Summary

We present a new implementation of least-squares reverse-time migration which accounts for the non-linear relationship between the data and reflectivity. As with other least-squares migration methods, the key feature of this approach is that it uses an approximation for the inverse of the modeling operator instead of its adjoint. However, in applying reverse-time migration, the two-way wave equation is used, which in turn provides a better approximation to the modeling operator. The approach described here is robust, and suitable for application in 3D.

Introduction

Migration attempts to produce an image of the subsurface by reversing the propagation effects in seismic data. Although in principle this requires the inverse of a modeling operator, in practice the adjoint of the modeling operator is used instead. This applies to nearly all migration methods, including reverse-time migration (RTM). In cases where the data are subject to significant aliasing, truncation, noise, or are incomplete, the adjoint of a modeling operator is not a good approximation to the inverse (Claerbout, 1992), and this degrades the resolution of the final migrated image.

An improved approximation to the inverse operator can be obtained using a least-squares approach (Nemeth et al., 1999; Kühl and Sacchi, 2001; Kaplan et al., 2010; Dai and Schuster, 2010). In practice, as in the matrix-based least-squares reverse-time migration of Yao and Jakubowicz (2012), it is normally assumed that the forward modeling and adjoint operators are linear with respect to reflectivity. In this paper we present an alternative formulation of least-squares reverse-time migration which generates the predicted data directly from the reflectivity without assuming linearity. We refer to this method as non-linear least-squares reverse-time migration (NLLSRTM).

Theory

Migration consists of three steps: forward modeling of the source wavefield, back propagation of the recorded data, and imaging. In conventional RTM, forward modeling is achieved by solving the two-way wave equation, and, for a point source, can be expressed as

$$u_s(\mathbf{x}, \omega) = G(\mathbf{x}|\mathbf{x}_s; \omega) S(\omega), \quad (1)$$

where u_s is the modeled wavefield, G is the Green's function, S is the source signature, \mathbf{x} is position, \mathbf{x}_s is the

source location, and ω is angular frequency. The recorded data, D , are then back-propagated into the subsurface using the adjoint of the modeling operator, G^\dagger , giving

$$u_r(\mathbf{x}, \omega) = \int G^\dagger(\mathbf{x}|\mathbf{x}_r; \omega) D(\mathbf{x}_r, \omega) d\mathbf{x}_r. \quad (2)$$

The imaging step generates an estimate of the reflectivity, $I(\mathbf{x})$, by relating u_s and u_r to each other at all points in the subsurface. This is usually done by correlating the wavefields and selecting the zero lag, and can be expressed in the frequency domain as

$$I(\mathbf{x}) = \int u_s(\mathbf{x}, \omega) u_r^\dagger(\mathbf{x}, \omega) d\omega, \quad (3)$$

where u_r^\dagger is the conjugate (time-reverse) of the back-propagated data. Substituting Equations 1 and 2 into Equation 3 then gives the basic equation of RTM:

$$I(\mathbf{x}) = \iint [G(\mathbf{x}|\mathbf{x}_s; \omega) S(\omega)] [G^\dagger(\mathbf{x}|\mathbf{x}_r; \omega) D(\mathbf{x}_r, \omega)]^\dagger d\omega d\mathbf{x}_r. \quad (4)$$

As discussed in Yao and Jakubowicz (2012), the use of crosscorrelation for imaging degrades the resolution in the migrated result. An alternative approach is to deconvolve the reflected wavefield by the incident wavefield (Valenciano and Biondi, 2003). This then gives

$$I(\mathbf{x}) = u_r(\mathbf{x}, \omega) / u_s(\mathbf{x}, \omega), \quad (5)$$

where the reflectivity is taken to be independent of frequency. However, while Equation 5 can provide better resolution than crosscorrelation, it also normally uses the adjoint of the forward-modeling operator, rather than its inverse. As a result, it still only provides an approximation to the reflectivity.

The true reflectivity, $R(\mathbf{x})$, is related to the incident and reflected wavefields by

$$u_r(\mathbf{x}, \omega) = u_s(\mathbf{x}, \omega) R(\mathbf{x}). \quad (6)$$

However, from Equation 2, the propagation from the reflection point to the receivers (modeling) can be expressed as

$$D(\mathbf{x}_r, \omega) = \int G(\mathbf{x}_r|\mathbf{x}; \omega) u_r(\mathbf{x}, \omega) d\mathbf{x}. \quad (7)$$

Inserting Equations 1 and 6 into Equation 7 then gives

$$D(\mathbf{x}_r, \omega) = \int G(\mathbf{x}_r|\mathbf{x}; \omega) R(\mathbf{x}) G(\mathbf{x}|\mathbf{x}_s; \omega) S(\omega) d\mathbf{x}. \quad (8)$$

NLLSRTM

Equation 8 describes the (exact) forward-modeling process which relates the true reflectivity to the data. It can be used to solve for the reflectivity using localized least-squares inversion by optimizing the objective function $\varphi_D(I(\mathbf{x}))$, where

$$\varphi_D(I(\mathbf{x})) = \frac{1}{2} \| \langle D(\mathbf{x}_r) \rangle - D(\mathbf{x}_r) \|^2, \quad (9)$$

and $\langle D(\mathbf{x}_r) \rangle$ and $D(\mathbf{x}_r)$ are respectively the predicted and recorded data. Converting Equation 8 into a matrix form, the gradient of the objective function with respect to I is then given by

$$\frac{\partial \varphi_D(I(\mathbf{x}))}{\partial I(\mathbf{x})} = \text{Re}\{[GS]^\dagger [G^\dagger (GI(\mathbf{x})GS - D(\mathbf{x}_r))] \}, \quad (10)$$

where "Re" indicates the real part of a complex number.

Equation 10 not only provides a means of calculating the gradient, but also gives it a physical meaning. In particular, GS describes the forward-propagated wavefield from the source, while $GI(\mathbf{x})GS - D(\mathbf{x}_r)$ is the data residual, and G^\dagger backward propagates the residual into the earth. Multiplication of $G^\dagger(GI(\mathbf{x})GS - D(\mathbf{x}_r))$ with the complex conjugate of GS is then equivalent to using the zero-lag crosscorrelation imaging condition. Equation 10 can be expressed in the time domain as

$$\frac{\partial \varphi_D(I(\mathbf{x}))}{\partial I(\mathbf{x})} = \sum_t [G^\dagger S^\dagger] * [(G * I(\mathbf{x}) * G * S - D) * G^\dagger], \quad (11)$$

where '*' denotes convolution.

Given the gradient of the objective function, the reflectivity model can be iteratively updated as

$$I_{n+1}(\mathbf{x}) = I_n(\mathbf{x}) + \alpha \mathbf{q}, \quad (12)$$

where α is an optimum step length, and \mathbf{q} is the update direction. In practice, the step length is determined using a linear search technique such as the secant method (Rajaraman, 2006). Since the gradient at each iteration is generated from solutions of the two-way wave equation, this provides a nonlinear relationship between the data and reflectivity models. We therefore refer to the method as nonlinear least-squares reverse-time migration. However, it should be noted that the updating scheme used for the iterative solution is still linear.

Implementation

The effectiveness of the migration can be enhanced using regularization in the optimization. In particular, if the recorded data are incomplete, or the data are contaminated by noise, NLLSRTM becomes an ill-posed problem, and

produces high-wavenumber artifacts. One way of reducing the artifacts is to use a roughness penalty constraint (Bube and Langham, 2008). In our implementation, this is done using first-order derivatives to measure the roughness of the model. Specifically, for the horizontal direction, the objective function of the roughness penalty constraint is

$$\varphi_h(I(\mathbf{x})) = \frac{1}{2} \|\partial_h I(\mathbf{x})\|^2, \quad (13)$$

where ∂_h is the first-order derivative along the horizontal direction; a similar roughness penalty constraint, $\varphi_v(I(\mathbf{x}))$, is also used for the vertical direction. Combining these constraints with the original objective function, and scaling the penalty terms by the trade-off parameters, λ_h and λ_v , then gives the final objective function as

$$\varphi = \varphi_D + \lambda_h \varphi_h + \lambda_v \varphi_v. \quad (14)$$

Because ∂_h and ∂_v are both well-posed, Equation 14 converts the ill-posed problem given by Equation 9 into a well-posed problem.

A second feature of our implementation is the option to weight later arrivals, and thereby enhance imaging of deeper reflectors. This increases the contributions of the late arrivals to the residual, and in turn affects the gradient, and updates, ultimately favoring the weighted terms. By contrast, the amplitudes of early events in seismic records are usually bigger than those for later events, and can otherwise dominate the calculation. Weighting the late arrivals also helps improve the speed of convergence.

Examples

We will demonstrate our implementation of LSRTM using two models. The first model consists of nine point diffractors embedded in a medium with a constant velocity of 2000 m/s (Figure 1a). Figure 1d shows a shot record from this model for a surface source at $x=450$ m, and receivers every 25 m along the surface; the source signature is a 30 Hz Ricker wavelet, and the direct arrivals, which do not contribute to imaging, have been removed. Figures 1b and 1c show the results of applying conventional RTM and NLLSRTM to the data in Figure 1d, while Figures 1e and 1f show the modeled data corresponding to the RTM and NLLSRTM images.

Figure 1 shows that NLLSRTM has two advantages relative to RTM. First, the diffractors in the NLLSRTM image have fewer sidelobes, and are better resolved than those from RTM. This is because the imaging condition for RTM is based on crosscorrelation, and therefore retains (actually amplifies) the imprint of the source signature. By contrast, in matching the image and recorded data,

NLLSRTM

NLLSRTM compensates for the source signature. Indeed, the compensation is equivalent to using the deconvolution imaging condition given by Equation 5 (Yao and Jakubowicz, 2012). Second, the amplitudes of the later arrivals in the modeled NLLSRTM data are closer to those in the recorded data than in the case of RTM. This is because RTM uses adjoint, rather than inverse, operators, and these fail to correct adequately for geometrical spreading. These advantages of NLLSRTM are intrinsic to the combination of least-squares imaging and reverse-time migration, and can be obtained with other implementations of LSRTM, including that of Yao and Jakubowicz (2012).

The second example uses the Marmousi model (Versteeg and Grau, 1991; Versteeg, 1993). Figure 2a shows a shot record at source location $x=3000$ m from the Marmousi model, with receivers located between 425 m and 2800 m at intervals of 12.5 m (the reflectivity model is shown in Figure 3a). Figure 2b shows the result of RTM after application of a Laplacian filter to remove low-wavenumber artifacts which are inherent in the solution of the two-way wave equation. Although Laplacian filtering removes the low-wavenumber artifacts, the RTM image retains high-wavenumber artifacts. By comparison, Figure 2c shows the result of NLLSRTM after Laplacian filtering. This image has fewer artifacts, is more highly resolved than that from RTM, and also has more consistent amplitudes over a wider area.

Figure 3 shows the reflectivity for the Marmousi model, together with stacks of the images obtained by migrating fifteen shots across the Marmousi model using different reverse-time migration techniques. Figure 3b is the result of conventional RTM after Laplacian filtering, while Figure 3c is that of LSRTM using the method of Yao and Jakubowicz (2012); Figure 3d is the result of NLLSRTM. In the case, for both the LSRTM and NLLSRTM results,

stacking attenuated the low-wavenumber artifacts, which in turn allowed the residuals to be removed using a mild low-pass filter. As might be expected from the results in Figure 2, the RTM result shows a noticeable decrease in amplitudes with depth because of inadequate correction for geometrical spreading. By contrast, the amplitudes in both the LSRTM and NLLSRTM results are both closer to those of the true reflectivity.

In principle, both LSRTM and NLLSRTM should give the same results. However, as is apparent in the examples shown here, they do have subtle differences. In particular, the results of NLLSRTM are somewhat cleaner than those for LSRTM. This is because the LSRTM uses separate calculations for the adjoint and modeling processes, and this can introduce artifacts and instabilities when the two results are not exact adjoints of each other (Claerbout, 1992). By contrast, by using direct least-squares inversion in combination with constraints, NLLSRTM can provide a stable and robust method of imaging. Moreover, whereas the LSRTM implementation of Yao and Jakubowicz (2012) is computationally relatively efficient, it requires a large amount of storage, and is currently impractical for application on 3D data. By contrast, the NLLSRTM method described here, while computationally more expensive, can be readily adapted for application on 3D data.

Conclusions

We have shown that NLLSRTM can be an effective method for seismic data migration. In particular, in addition to retaining the benefits of least-squares imaging within the framework of reverse-time migration, it is robust and stable, and is suitable for application in 3D.

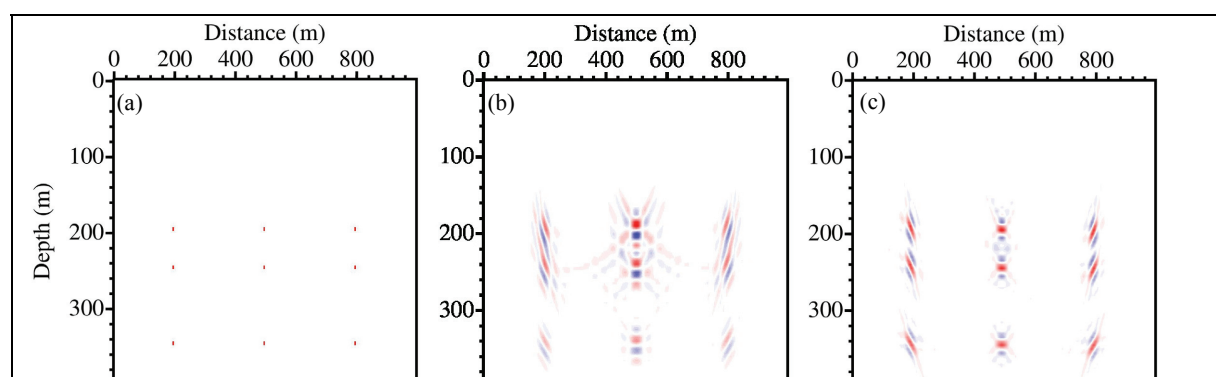
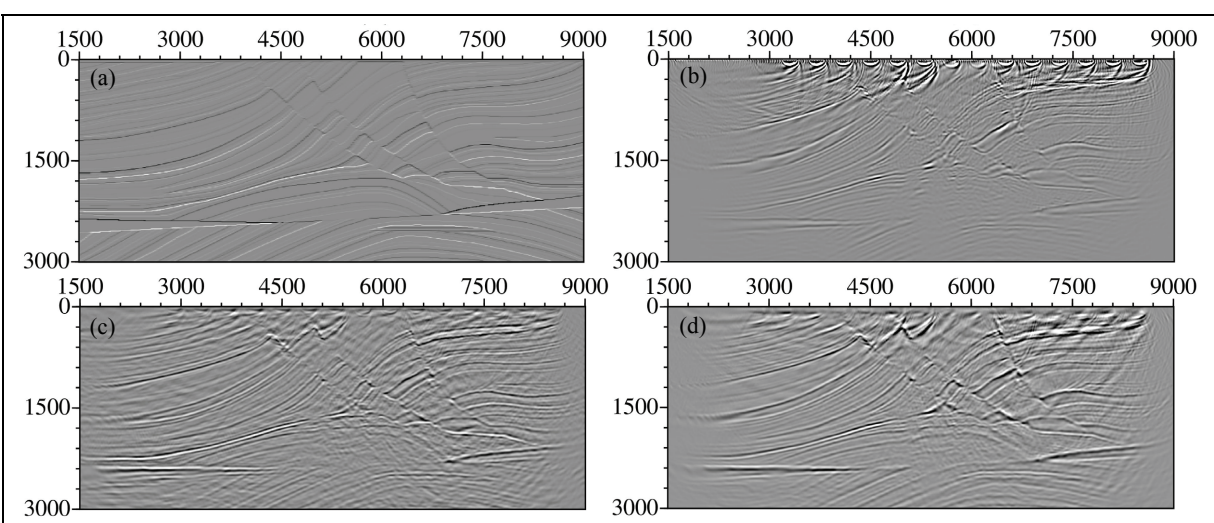
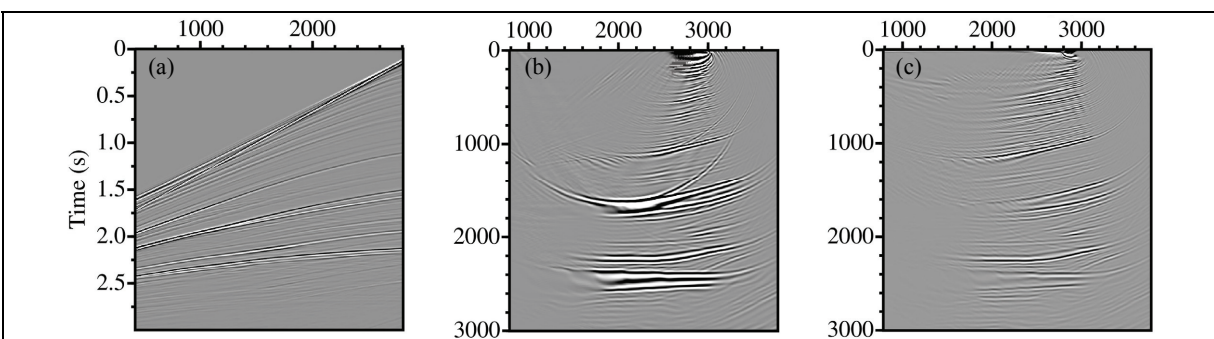
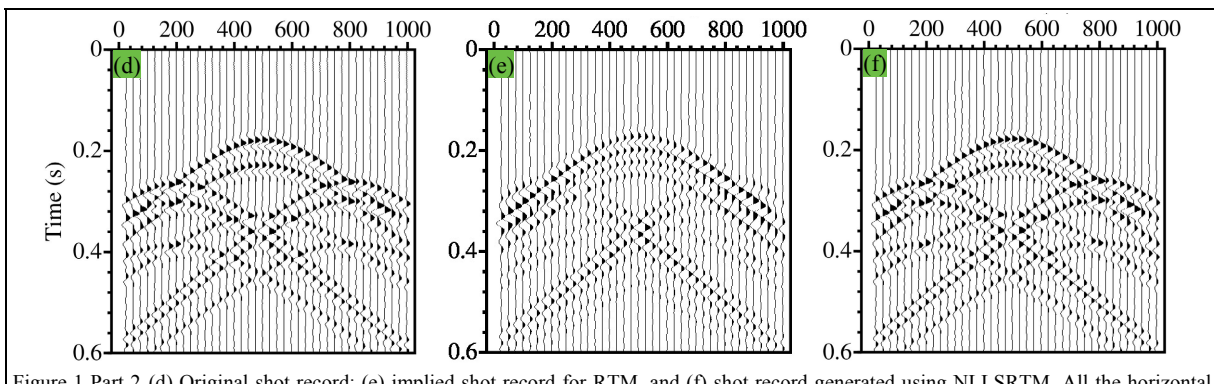


Figure 1 Part 1 (a) Model containing nine point diffractors embedded in a medium with a constant velocity of 2000 m/s; (b) RTM for a shot record from the model shown in (a), and (c) the same as (b) but using NLLSRTM.

NLLSRTM

<http://dx.doi.org/10.1190/segam2012-1435.1>

EDITED REFERENCES

Note: This reference list is a copy-edited version of the reference list submitted by the author. Reference lists for the 2012 SEG Technical Program Expanded Abstracts have been copy edited so that references provided with the online metadata for each paper will achieve a high degree of linking to cited sources that appear on the Web.

REFERENCES

- Bube, K. P., and R. T. Langan, 2008, A continuation approach to regularization of ill-posed problems with application to crosswell-traveltime tomography: *Geophysics*, **73**, no. 5, VE337-VE351.
- Claerbout, J. F., 1992, *Earth soundings analysis: Processing versus inversion*: Blackwell Science.
- Dai, W., and G. T. Schuster, 2010, Multi-source wave-equation least-squares migration with a deblurring filter: 72nd Conference and Exhibition, EAGE, Extended Abstracts, P276.
- Kaplan, S. T., P. S. Routh, and M. D. Sacchi, 2010, Derivation of forward and adjoint operators for least-squares shot-profile split-step migration: *Geophysics*, **75**, no. 6, S225-S235.
- Kühl, H., and M. D. Sacchi, 2001, Generalized least-squares DSR migration using a common angle imaging condition: 71st Annual International Meeting, SEG, Expanded Abstracts, 1025-1028.
- LeBras, R., and R. W. Clayton, 1988, An iterative inversion of back-scattered acoustic waves: *Geophysics*, **53**, 501-508.
- Nemeth, T., C. Wu, and G. T. Schuster, 1999, Least-squares migration of incomplete reflection data: *Geophysics*, **64**, 208-221.
- Rajaraman, V., 2006, Computer oriented numerical methods: Prentice-Hall of India.
- Valenciano, A. A., and B. Biondi, 2003, 2-D deconvolution imaging condition for shot-profile migration: 73rd Annual International Meeting, SEG, Expanded Abstracts, 1059-1062.
- Versteeg, R. J., 1993, Sensitivity of prestack depth migration to the velocity model: *Geophysics*, **58**, 873-882.
- Versteeg, R. J., and G. Grau, eds., 1991, The Marmousi experience: EAGE, workshop on practical aspects of seismic data inversion (Copenhagen, 1990).
- Yao, G., and H. Jakubowicz, 2012, Least-squares reverse-time migration: Abstract submitted for presentation at the 82nd Annual International Meeting, SEG.